https://doi.org/10.1016/j.jlumin.2019.116963

Efficient TADF-OLEDs with Ultra-soluble Copper(I) Halide Complexes Containing Non-Symmetrically Substituted Bidentate Phosphine and PPh_3 Ligands

Bang-Ke Guo[a], Fei Yang[b], Ya-Qi Wang[a], Qiong Wei[a], Li Liu[a*], Xin-Xin Zhong[a*], Lei Wang[b*], Jian-Kang Gong[a], Fa-Bao Li[a], Wai-Yeung Wong[c*], Khalid A. Alamry[d], Yi Zhao[e]

[a] *Hubei Collaborative Innovation Center for Advanced Organic Chemical Materials, Ministry of Education Key Laboratory for the Synthesis and Application of Organic Functional Molecules, School of Chemistry and Chemical Engineering, Hubei University, Wuhan 430062, P. R. China. E-mail: liulihubei@hubu.edu.cn; xxzhong@hubu.edu.cn*

[b] *Wuhan National Laboratory for Optoelectronics, Huazhong University of Science and Technology, Wuhan 430074, P. R. China. E-mail: wanglei@mail.hust.edu.cn*

[c] Department of Applied Biology and Chemical Technology, The Hong Kong Polytechnic University, Hung Hom, Hong Kong, P. R. China. *E-mail: wai-yeung.wong@polyu.edu.hk*

[d] *Chemistry Department, Faculty of Science, King Abdulaziz University, Jeddah 21589, Saudi Arabia.*

[e] *State Key Laboratory of Physical Chemistry of Solid Surfaces, Xiamen University, Xiamen 361005, P. R. China.*

Bang-Ke Guo, Fei Yang and Ya-Qi Wang contributed equally to this work.

Abstract

High efficiency copper(I) halide complexes containing rigid diphosphine ligand have attracted much attention. However, rigid bidentate phosphine ligands were rarely reported so far and limited to structural symmetric diphosphines. Here, a series of

four-coordinate mononuclear copper(I) halide complexes containing non-symmetrically substituted bidentate phosphine and PPh_3 Ligands, $CuX(dpts)(PPh_3)$ [dpts = 2-trimethylsilyl-3,4-bis(diphenylphosphine)thiophene, X = I (**1**), Br (**2**), Cl (**3**)] and in comparison to $CuX(dppt)(PPh_3)$ [dppt = 3,4-bis(diphenylphosphino)thiophene, X = I (**4**), Br (**5**), Cl (**6**)], were synthesized, and their molecular structures and photophysical properties were investigated. The introduction of trimethylsilyl group into diphosphine ligand, not only greatly improves the solubility of the complexes, but also quantum efficiency, and fine-tunes the emission color as well. These complexes exhibit intense bluegreen to yellowish green emissions in powder state at room temperature and have peak wavelengths at 485–535 nm with microsecond lifetimes (τ = 4.8–48.9 μs, Φ = 0.03–0.52). The emission of the complexes **1–6** mainly originates from MLCT (metal to ligand charge transfer), XLCT (halide to ligand charge transfer) and intraligand transitions. Solution-processed, nondoped and doped devices of complex **2** exhibit yellow green emission with CIE(x,y) of (0.43, 0.51). The nondoped device gives a maximum external quantum efficiency (EQE) of 7.74 % and a maximum luminance of 234 cd/m^2. These promising results open the door to solution-processed, efficient TADF (thermally activated delayed fluorescence) OLED (organic light-emitting diode) devices with ultra-soluble and abundant copper emitters.

Keywords: Mononuclear; Copper(I) halide complexes; Ultra-soluble; TADF; Bidentate phosphine.

1. Introduction

Phosphorescent complexes of noble metals, such as iridium, have attracted much attention due to their potential applications as organic light-emitting diodes (OLEDs) [1-5]. As an attractive alternative to expensive and less abundant heavy metals, luminescent Cu(I) complexes have become popular over the past few decades [6-16]. This opens the door to large-scale fabrication of OLED. The low lying MLCT excited states and small singlet-triplet energy gap (ΔE_{ST}), can effectively harvest triplet excitons for thermally activated delayed fluorescence (TADF) emission [17-19]. With the capability to harvest both the singlet and triplet excitons, the Cu(I) complexes with TADF have been regarded as promising emitters in electroluminescent devices [20-21].

Recently, TADF materials based on neutral Cu(I) halide complexes with different structural motifs, such as tetrahedral or trigonal coordinated mono-, di- and multinuclear Cu(I) complexes have been studied [22-26]. A three-coordinate Cu(I) halide complex reported by Osawa et al. gave the external quantum efficiency (EQE) over 20% in vacuum-deposited OLEDs [23,24]. Comparing with most literatures dealing with vacuum-processed devices, there are only a few reports on neutral Cu(I) halide complexes fabricated as OLEDs by industrial solution-processing techniques [27-32].

TADF materials are often too insoluble to allow the solution-processed devices prepared by spin-coating. Based on our previous work [33], in order to increase the

solubility of the materials, we used a non-symmetrically substituted diphosphine ligand 2-trimethylsilyl-3,4-bis(diphenylphosphine)thiophene (dpts) to increase the solubility of the materials (Scheme 1). The introduction of flexible and electron-donating group trimethylsilyl into 3,4-bis(diphenylphosphine)thiophene (dppt), not only increases the solubility of Cu(I) halide complexes, but also quantum efficiency and fine-tunes the emission maxima. We report here a series of neutral luminescent mononuclear four-coordinate copper(I) halide complexes CuX(dpts)(PPh_3) [dpts = 2-trimethylsilyl-3,4-bis(diphenylphosphine)thiophene, X = I (**1**), Br (**2**), Cl (**3**)] and CuX(dppt)(PPh_3) [dppt = 3,4-bis(diphenylphosphino)thiophene, X = I (**4**), Br (**5**), Cl (**6**)]. Their molecular structures and photophysical properties were investigated.

2. Experimental section

2.1.Materials

All starting chemicals and reagents are of commercial reagent grade. Ligands 2-trimethylsilyl-3,4-bis(diphenylphosphine)thiophene (dpts) and 3,4-bis(diphenylphosphino)thiophene (dppt) were synthesized according to the literature method [34-35].

2.2.Instrumentation

^{1}H, ^{13}C and ^{31}P NMR in $CDCl_3$ spectra were recorded using a Varian 600 or 500 MHz NMR spectrometer. High resolution mass spectra (HRMS) were

recorded on the Thermo Scientific Exactive Plus equipped with ESI ionization source. C and H analyses were determined using a Vario Micro Cube elemental analyzer. The single crystal structures of the complexes **1**–**6** were measured using a XtaLAB Synergy, Dualflex, HyPix or photo-100 CMOS area detector diffractometer. UV–vis absorption and emission spectra were recorded by a Unicam Helios α spectrometer and a FLS920 steady state & time-resolved fluorescence spectrometer, respectively. Solid-state Φ_{PL} values were determined with an absolute PL quantum yield measurement system (Hamamatsu). The PL lifetimes were measured by a single photon counting spectrometer with a Picosecond Pulsed UVLASTER (LASTER377) as the excitation source. Thermogravimetric analysis (TGA) was performed on a thermal analysis instrument (Perkin-Elmer Diamond).

2.3.Synthesis of complexes 1-6

All Cu(I) complexes were synthesized according to the similar procedure in literature [33b].

[CuI(dpts)(PPh_3)] (1). Greenish-yellow crystals (Yield: 310.6 mg, 83.4%). ^{1}H NMR (500 MHz, $CDCl_3$) δ: 7.90-7.67 (m, 3H), 7.62 (s, 1H), 7.23-7.00 (m, 24H), 6.90-6.70 (m, 8H), -0.21 (s, 9H). ^{31}P NMR (200 MHz, $CDCl_3$) δ: 3.99 (s, PPh_3), -14.90 (d, J = 168 Hz, 4-PPh_2), -22.02 (d, J = 164 Hz, 3-PPh_2). Anal. Calcd for $C_{49}H_{45}CuIP_3SSi$: C, 60.21; H, 4.64. Found: C, 60.26; H, 4.60. HRMS (ESI): m/z calcd for $[C_{49}H_{45}CuP_3SSi]^+$, 849.1520. Found: 849.1547.

[CuBr(dpts)(PPh_3)] (2). Greenish-yellow crystals (Yield: 294.0 mg, 82.9%). ^{1}H

NMR (500 MHz, $CDCl_3$) δ: 7.92-7.73 (m, 4H), 7.59 (t, J = 5 Hz, 1H), 7.33-7.27 (m, 4H), 7.23 (t, J= 7.5 Hz, 5H), 7.17-7.00 (m, 15H), 6.90-6.65 (m, 7H), -0.22 (s, 9H). ^{31}P NMR (200 MHz, $CDCl_3$) δ: 5.20 (s, PPh_3), -13.44 (d, J = 136 Hz, 4-PPh_2), -20.81 (d, J = 132 Hz, 3-PPh_2). Anal. Calcd for $C_{49}H_{45}BrCuP_3SSi$: C, 63.25; H, 4.88; Found: C, 63.29; H, 4.84. HRMS (ESI): m/z calcd for $[C_{49}H_{45}CuP_3SSi]^+$, 849.1520, found: 849.1548.

[CuCl(dpts)(PPh_3)] (3). Greenish-yellow crystals（Yield: 269.5 mg, 79.8%）. ^1H NMR (500 MHz, $CDCl_3$) δ: 7.97-7.75 (m, 4H), 7.57 (t, J = 5 Hz, 1H), 7.33-7.27 (m, 4H), 7.21 (t, J = 7.5 Hz, 4H), 7.15-7.00 (m, 15H), 6.90-6.60 (m, 8H), -0.23 (s, 9H). ^{31}P NMR (200 MHz, $CDCl_3$) δ: 5.96 (s, PPh_3), -12.56 (d, J = 150 Hz, 4-PPh_2), -20.03 (d, J = 150 Hz, 3-PPh_2). Anal. Calcd for $C_{49}H_{45}ClCuP_3SSi$: C, 66.43; H, 5.12; Found: C, 66.47; H, 5.10. HRMS (ESI): m/z calcd for $[C_{49}H_{45}CuP_3SSi]^+$, 849.1520, found: 849.1549.

[CuI(dppt)(PPh_3)] (4). Colorless crystals (Yield: 1.633 g, 81.6%). ^1H NMR (600 MHz, $CDCl_3$) δ: 7.80–7.70 (m, 3H), 7.38 (t, *J* = 6 Hz, 2H), 7.30–7.15 (m, 16H), 7.15–7.00 (m, 9H), 6.93–6.85 (m, 4H), 6.80–6.70 (m, 3H). ^{31}P NMR (240 MHz, $CDCl_3$) δ: –2.55 (s), –27.36 (s). Anal. Calcd for $C_{46}H_{37}CuIP_3S$: C, 61.03; H, 4.12. Found: C, 61.07; H, 4.09. HRMS (ESI): m/z calcd for $[C_{46}H_{37}CuP_3S]^+$, 777.1125, found: 777.1080.

[CuBr(dppt)(PPh_3)] (5). Colorless crystals (Yield: 1.531 g, 80.7%). ^1H NMR (600 MHz, $CDCl_3$) δ: 7.88–7.78 (m, 3H), 7.34 (t, *J* = 6 Hz, 2H), 7.30–7.17 (m, 16H),

7.17–7.00 (m, 9H), 6.95–6.80 (m, 4H), 6.78–6.70 (m, 3H). ^{31}P NMR (240 MHz, $CDCl_3$) δ: –1.18 (s), –25.99 (s). Anal. Calcd for $C_{46}H_{37}CuBrP_3S$: C, 64.38; H, 4.35. Found: C, 64.40; H, 4.32. HRMS (ESI): m/z calcd for $[C_{46}H_{37}CuP_3S]^+$, 777.1125, found: 777.1036.

[CuCl(dppt)(PPh_3)] (6). Colorless crystals (Yield: 1.463 g, 81.3%). ^{1}H NMR (600 MHz, $CDCl_3$) δ: 7.95–7.80 (m, 3H), 7.33 (t, *J* = 6 Hz, 2H), 7.30–7.15 (m, 16H), 7.08–7.05 (m, 9H), 6.95–6.80 (m, 4H), 6.76–6.65 (m, 3H). ^{31}P NMR (240 MHz, $CDCl_3$) δ: –0.08 (s), –25.08 (s). Anal. Calcd for $C_{46}H_{37}CuClP_3S$: C, 67.89; H, 4.58. Found: C, 67.86; H, 4.55. HRMS (ESI): m/z calcd for $[C_{46}H_{37}CuP_3S]^+$, 777.1125, found: 777.0949.

3. Results and discussion

3.1.Description of syntheses and structures

The synthetic routes of the Cu(I) complexes are depicted in Scheme 1. The mononuclear complexes [CuX(dpts)PPh_3] (X = I for **1**, Br for **2**, Cl for **3**) and CuX(dppt)(PPh_3) [X = I (**4**), Br (**5**), Cl (**6**)] were prepared in 79.8–83.4% yield via the addition of PPh_3 to a mixture of CuX in dichloromethane with dpts and dppt, respectively. All the new Cu(I) complexes readily dissolve in general solvents such as dichloromethane, acetonitrile and DMSO. Their structures were characterized and confirmed by HRMS spectrometry, single crystal X-ray diffraction, and NMR spectroscopy. In order to investigate the effect of the introduction of trimethylsilyl group on the solubility of the complexes, we select complexes **2** and **5** as

representative samples to compare the solubility in various solvents. As it is given in Table 1, the solubility of complex **2** in various solvents used is remarkably larger than complex **5**. The solubility in the low boiling point polar solvent acetonitrile and high boiling point polar solvents diethyl phthalate and DMSO is in the order of 30, 80 and more than 100 mg mL^{-1}, respectively. The solubility in unpolar solvents is of particular interest: For the high boiling point solvents chlorobenzene, tetralin and toluene, solubility values of more than 100 mg mL^{-1} were found. With this broad solubility in various solvents, it is possible to create high-performance inks that can be adjusted to various print heads by using solvent mixtures.

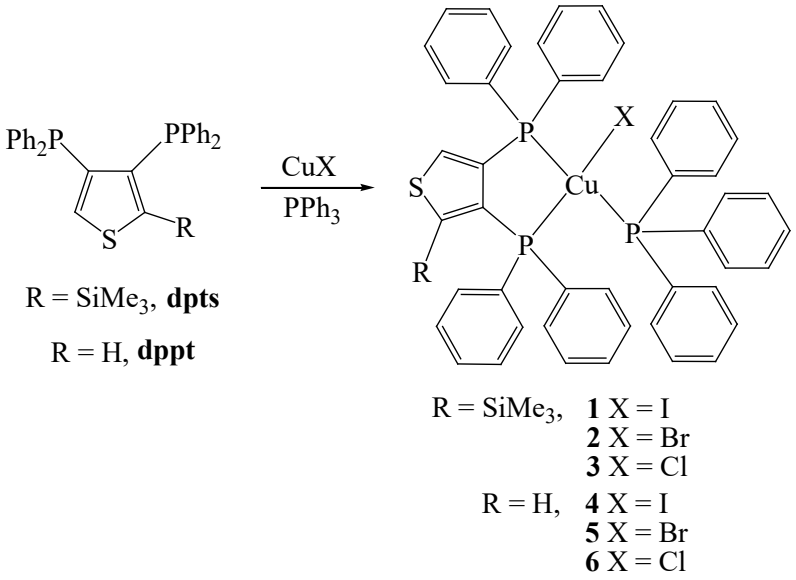

Scheme 1. Synthetic pathways to mononuclear copper(I) complexes.

Table **1**. Solubility data for complexes **2** and **5** in various solvents.

Solvent	Solubility (mg mL^{-1})	
	2	**5**
Chlorobenzene	>100	70–80
DMSO	>100	50

Acetonitrile	20–30	<5
Ethanol	4–5	<1
Mesitylene	8–10	2–3
Tetralin	>100	5–10
Toluene	>100	5–10
Diethyl phthalate	70–80	5–10

3.2.X-ray crystallographic study

ORTEP diagrams of **1**-**6** are shown in Fig.1. Crystallographic data and selected bond lengths and angles are collected in Tables 2 and 3, respectively. In these complexes, each of the copper(I) atoms coordinated with three phosphorous and one halogen atom; these d^{10} centers located in a highly distorted tetrahedral environment. The P_{diphos}–Cu–P_{diphos} angles of complexes **1-3**, ranging from 84.44 to 89.80°, are a little larger than the angles ranging from 89.98 to 91.20° for complexes **4-6**, possibly due to the steric hindrance by bulky trimethylsilyl near to the PPh_2 on thiophene ring. As listed in Table 2, the Cu–X distances of complexes **1**-**6** elongate with an increase in the van der Waals radius of X. Intermolecular hydrogen bonds between the halide of **2** and **3** to the hydrogens of the dpts diphenylphosphino phenyl rings are observed; the closest of these Br-H and Cl-H separations are 2.929 and 2.853 Å. Since there are 5 solvent CH_2Cl_2 molecules in the structure of complex **5**, intermolecular hydrogen bond between H of CH_2Cl_2 to Br of complex can be observed, with the closest Br-to-H distance is 2.854 Å. Complex **1-6** show intermolecular C–H π interactions between the methyl of trimethylsilyl and PPh_3 phenyl rings for **1**, PPh_3 phenyl rings

for **2**,**4** and **6**, the dpts diphenylphosphino phenyl rings for **3**, the dppt diphenylphosphino phenyl rings and PPh_3 phenyl rings for **5**, with the closest C-to-H distances of 2.913, 2.809, 2.896, 2.828, 2.856 and 2.358 Å for **1-6**, respectively (supporting information Fig.S19-S24). Overall, all these intermolecular interactions are incorporated into 1-D tape-like arrays along the *b*-axis for **2, 3, 4** and **6,** and *a*-axis for **1, 2, 3** and **5**, respectively.

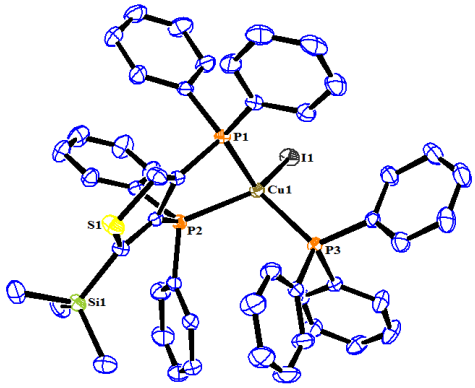

1

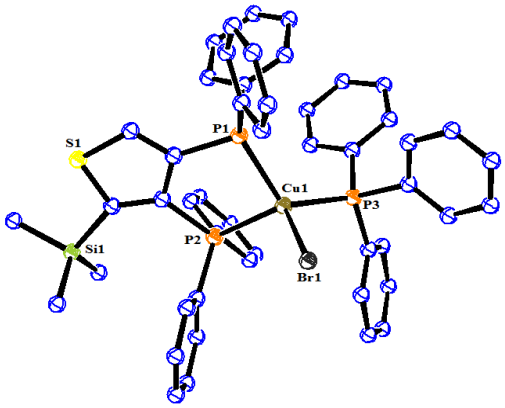

2

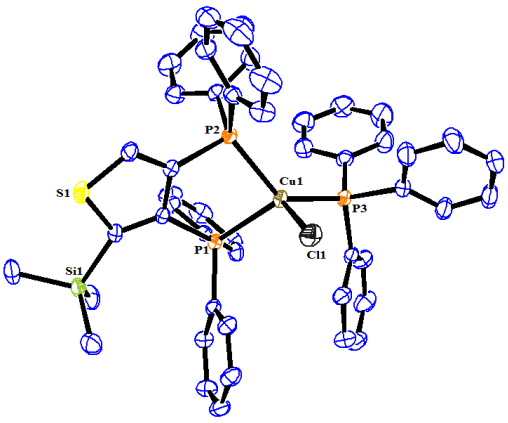

3

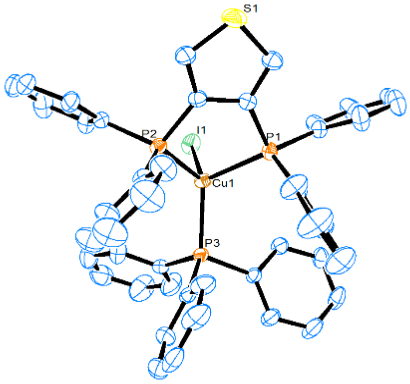

4

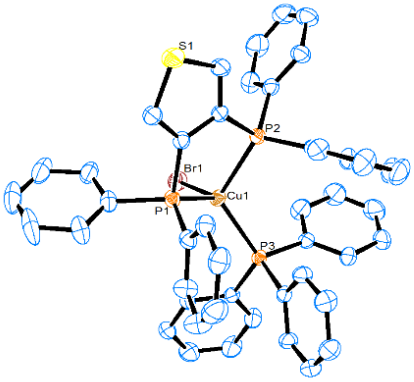

5

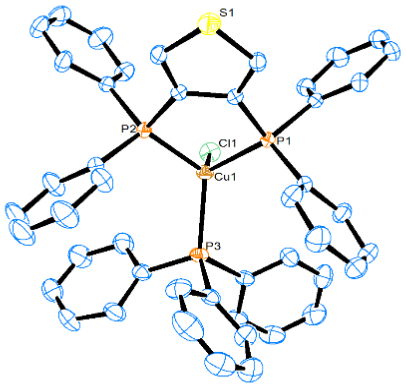

6

Fig.1. ORTEP diagrams of complexes **1-6.**

Table 2. Crystallographic data and refinement details for **1-6**.

	1	**2**	**3**
Empirical formula	$C_{49}H_{45}CuIP_3SSi$	$C_{49}H_{45}BrCuP_3SSi$	$C_{49}H_{45}ClCuP_3SSi$
Formula weight	977.35	930.36	885.90
Temperature (K)	293.0	293(2)	293
Wavelength (Å)	0.71073	1.54184	1.54184
Crystal system	Monoclinic	Monoclinic	Triclinic
Space group	P 1 21/n 1	P 21	P -1
a (Å)	10.7566(3)	18.05330(10)	10.4663(2)
b (Å)	41.3386(11)	11.28750(10)	12.4850(2)
c (Å)	10.9361(4)	22.6028(2)	18.9835(3)
V (Å^3)	4545.7(3)	4555.15(6)	2253.08(7)
Z	4	4	2
ρ (g cm^{-3})	1.428	1.357	1.306
μ (mm^{-1})	1.370	3.625	3.171
F (0 0 0)	1984	1912	920

θ range for data collection (°)	1.971 to 26.372	2.475 to 67.078	2.380 to 67.080
Index ranges	$-13 \le h \le 11$	$-18 \le h \le 21$	$-12 \le h \le 12$
	$-50 \le k \le 50$	$-13 \le k \le 13$	$-14 \le k \le 13$
	$-13 \le l \le 13$	$-27 \le l \le 27$	$-21 \le l \le 22$
Independent reflections	9156 [R(int) = 0.0453]	16246 [R(int) = 0.0698]	8046 [R(int) = 0.0431]
Completeness to θ = 25.242°	99.9%	100.0 %	99.9%
Max. and min. transmission	1.00000 and 0.39726	1.00000 and 0.39648	1.00000 and 0.43143
Gof	1.039	1.007	1.067
Final R indices [I > 2σ(I)]	R_1 = 0.0312	R_1 = 0.0381	R_1 = 0.0362
	wR_2 = 0.0693	wR_2 = 0.0982	wR_2 = 0.0942
R (all data)	R_1 = 0.0422	R_1 = 0.0406	R_1 = 0.0422
	wR_2 = 0.0729	wR_2 = 0.1030	wR_2 = 0.1002
Max/min (e Å^3)	0.401 and –0.600	0.287 and –0.580	0.333 and –0.353

	4	4 (**5**) • 5 (CH_2Cl_2)	**6**
Empirical formula	$C_{46}H_{37}CuIP_3S$	4 ($C_{46}H_{37}CuBrP_3S$) • 5 (CH_2Cl_2)	$C_{46}H_{37}CuClP_3S$
Formula weight	905.17	3857.33	813.72
Temperature (K)	297(2)	296(2)	297(2)
Wavelength (Å)	0.71073	0.71073	0.71073
Crystal system	Monoclinic	Monoclinic	Monoclinic
Space group	P 21/c	P 21/n	P 21/c
a (Å)	12.3705(13)	12.8387(18)	20.7532(29)
b (Å)	18.4017(20)	13.3034(20)	8.9378(14)
c (Å)	18.2837(20)	30.5816(46)	22.8230(38)
V (Å^3)	4132.6(8)	5213.2(13)	4030.5(11)
Z	4	1	4
ρ (g cm^{-3})	1.455	1.229	1.341

μ (mm^{-1})	1.474	1.474	0.811
F (0 0 0)	1824	1962	1680
θ range for data collection (°)	2.48 to 27.60	2.33 to 27.60	2.50 to 27.54
Index ranges	$-16 \le h \le 14$	$-16 \le h \le 16$	$-26 \le h \le 26$
	$-23 \le k \le 23$	$-17 \le k \le 17$	$-11 \le k \le 11$
	$-23 \le l \le 23$	$-39 \le l \le 39$	$-29 \le l \le 29$
Independent reflections	9535 [R(int) = 0.0376]	11955 [R(int) = 0.0474]	9285 [R(int) = 0.0625]
Completeness to θ = 27.60°	99.5 %	98.8 %	99.8%
Max. and min. transmission	0.6831 and 0.6662	0.7187 and 0.6044	0.7456 and 0.6930
Gof	1.029	1.055	1.053
Final R indices	R_1 = 0.0334,	R_1 = 0.0641	R_1 = 0.0398
[I > 2σ(I)]	wR_2 = 0.0716	wR_2 = 0.1873	wR_2 = 0.0830
R (all data)	R_1 = 0.0508	R_1 = 0.0960	R_1 = 0.0642
	wR_2 = 0.0786	wR_2 = 0.2116	wR_2 = 0.0918
Max/min (e Å^3)	1.095 and –1.190	1.437 and –0.453	0.316 and –0.483

Complex	**1**	**2**	**3**
Cu–X	2.6084(3)	2.4129(7), 2.4277(8)	2.3030(6)
Cu–P_{diphos}	2.2970(6)	2.2894(12), 2.3000(11)	2.3248(5)
	2.3317(6)	2.2912(12) 2.2812(13)	2.2756(5)
Cu–P_{PPh3}	2.2820(7)	2.2740(13), 2.2579(13)	2.2586(6)
P_{diphos}–Cu–P_{diphos}	84.44(2)	89.56(4), 89.80(4)	89.115(19)
P_{diphos}–Cu–P_{PPh3}	118.58(3)	118.84(5),119.29(5)	115.59(2)
	113.83(2)	117.52(5), 119.29(5)	128.15(2)

P_{diphos}–Cu–X	119.594(19)	109.20(4), 114.08(4)	109.03(2)
	115.04(2)	108.65(4), 117.04(4)	109.98(2)
P_{PPh3}–Cu–X	104.829(19)	105.47(4), 104.54(4)	104.02(3)

Table 3. Selected bond lengths [Å] and angles (°) for complexes **1-6**.

Complex	**4**	4 (**5**) • 5 (CH_2Cl_2)	**6**
Cu–X	2.6244(4)	2.4331(7)	2.3078(7)
Cu–P_{diphos}	2.3010(7), 2.3040(8)	2.2952(11), 2.3118(10)	2.2786(6), 2.2858(6)
Cu–P_{PPh3}	2.2643(7)	2.2720(10)	2.2804(7)
P_{diphos}–Cu–P_{diphos}	89.97(3)	90.45(4)	91.20(2)
P_{diphos}–Cu–P_{PPh3}	121.96(3), 117.51(3)	120.12(4), 115.55(4)	116.84(2), 117.44(2)
P_{diphos}–Cu–X	111.95(2), 108.39(2)	112.52(3), 112.63(3)	115.08(2), 114.75(2)
P_{PPh3}–Cu–X	106.12(2)	105.40(3)	102.29(2)

3.3.Photophysical properties

The absorption spectra of dpts, dppt, PPh_3 and complexes **1-6** in CH_2Cl_2 at room temperature are shown in Fig.2. The absorption spectra of dpts, dppt and PPh_3 display broad and intense bands at 255 nm ($\varepsilon = 2.07\times10^4$ M^{-1} cm^{-1}), 271 ($\varepsilon = 1.60 \times 10^4$ M^{-1} cm^{-1}) and 278 nm ($\varepsilon = 1.04\times10^4$ M^{-1} cm^{-1}), respectively, that can be assigned to a mixed transition of n→π* and π→π* of thienylphosphine and phenylphosphine compound. The absorption band maxima of dpts is blue-shifted about 16 nm than dppt. The introduction of one trimethylsilyl to diphosphine ligand, results in the structural asymmetry and decreased conjugation in the whole molecule. Complexes **1-3** have broad bands with maxima at 253-257 nm[$\varepsilon = (2.25 \sim 2.76) \times 10^4$ M^{-1} cm^{-1}], and broad shoulders at 280-297 nm [$\varepsilon = (1.97 \sim 2.33) \times 10^4$ M^{-1} cm and weaker band tails are

330-390 nm, and complexes **4-6** have red-shifted broad bands with maxima at 269-280 nm[ε = (1.99 ~ 2.04) × 10^4 M^{-1} cm^{-1}], broad shoulders at 305 nm [ε = (1.36 ~ 1.44) × 10^4 M^{-1} cm^{-1}], and weaker band tails are 333-395 nm. The weaker band tails may be due to the electronic transition being affected by the copper ions, the halide ligands, or both, or intraligand charge transfer (n→π*, π→π* or both). Our TDDFT (time-resolved density function theory) calculation on the absorption spectra of complexes **1-6** in CH_2Cl_2 are indicated in Figs.S38-S43 in supporting information, which are consistent with the experimental results. Based to the excitation properties (Tables S2-S7) for complexes **1-6**, the main contributions to the lowest excited states are the transitions from the highest occupied molecular orbital (HOMO) to the lowest unoccupied molecular orbital (LUMO). As shown in Fig.3, the HOMO electrons are mainly focused on the copper, halogen and P atoms in dpts, while the LUMO is mainly localized on the thiophenyl rings in dpts. We can thus conclude that the lowest excited states of complexes **1–6** consist of MLCT, XLCT and intraligand transitions, quite different from those in Cu(I) halides complexes [CuX(dpmt)(PPh_3)] containing diphosphine ligand dpmt (3,4-bis(diphenylphosphino)-2,5-dimethylthiophene) in which the lowest excited states consist of intraligand and LLCT (ligand to ligand charge transfer) transitions [33b].

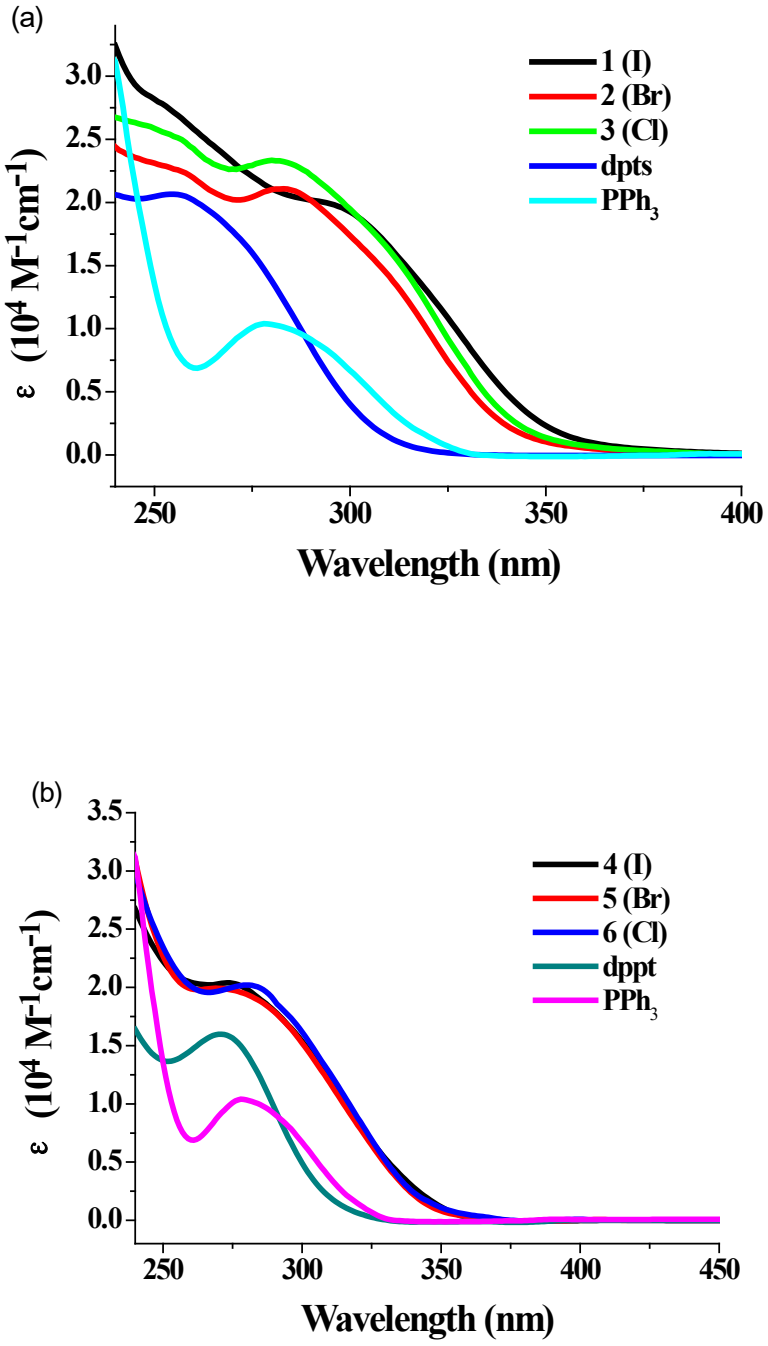

Fig.2. Absorption spectra of (a) dpts and PPh_3 and complexes **1-3** (b) dppt and PPh_3 and complexes **4-6** in CH_2Cl_2 at r.t.

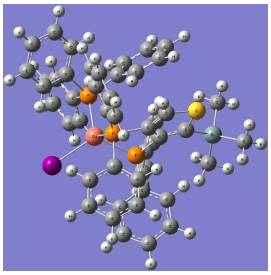

The optimized S_0 geometry

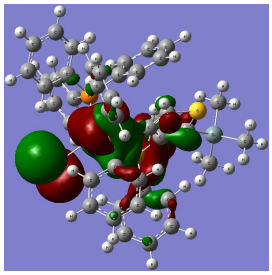

HOMO E = –5.55 eV

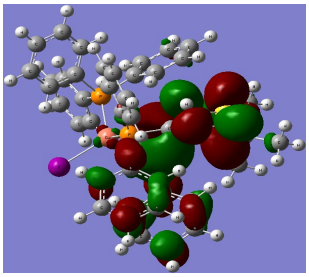

LUMO E = –1.61 eV

1

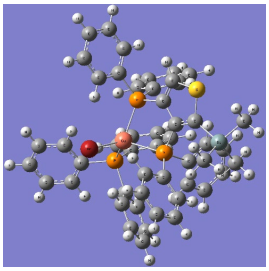

The optimized S_0 geometry

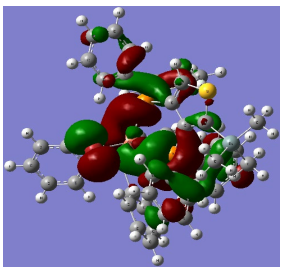

HOMO E = –5.59 eV

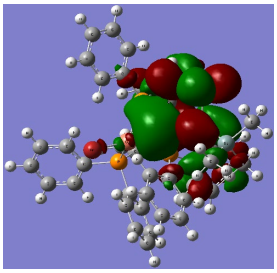

LUMO E = –1.58 eV

2

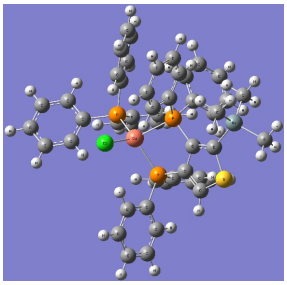

The optimized S_0 geometry

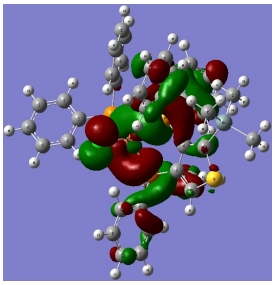

HOMO E = –5.58 eV

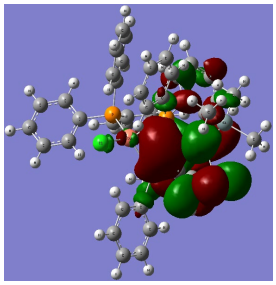

LUMO E = –1.56 eV

3

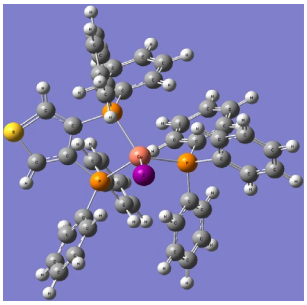

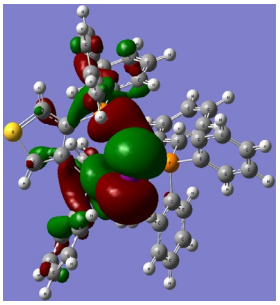

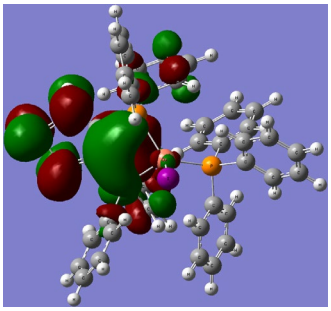

The optimized S_0 geometry HOMO E = –5.68 eV LUMO E = –1.52 eV

4

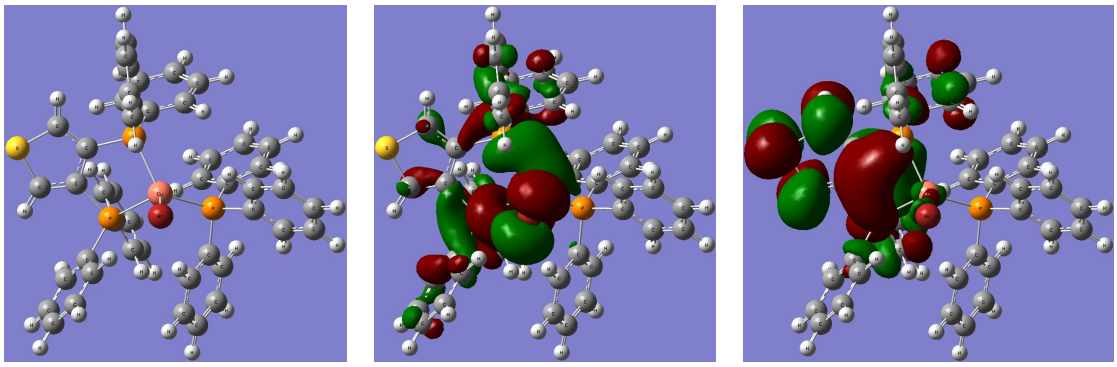

The optimized S_0 geometry HOMO E = –5.71 eV LUMO E = –1.51 eV

5

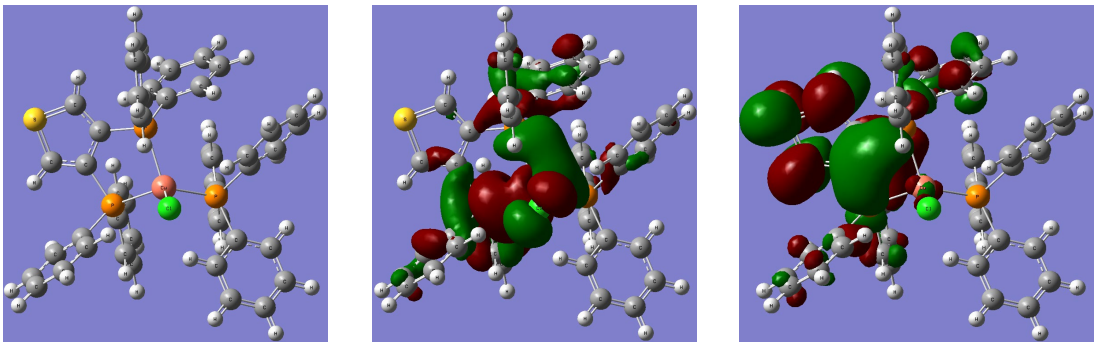

The optimized S_0 geometry HOMO E = –5.68 eV LUMO E = –1.58 eV

6

Fig.3. The optimized S_0 geometry, electron cloud distribution of HOMO and LUMO for complexes **1-6**.

The emission spectra of complexes **1-6** in the powder state measured at 297 K and 77 K are shown in Fig.4. Summarized in Table 4 are the emission maxima, lifetimes and quantum yields of the complexes at 297 and 77 K. Complexes **1-6** exhibit strong bluegreen to yellowish green emissions between 485 and 535 nm at

room temperature (λ_{ex}= 360 for **1-3**, 373 nm for **4-6)**. The quantum yields of **1-3** (Φ_{PL} = 0.29~0.52) are much higher than **4-6** (Φ_{PL} = 0.03~0.18). These emission bands are broad and unstructured, suggesting that the emissive excited states have charge-transfer character [16]. The emission bands of complexes **1** and **2** are blue-shifted by approximately 30 nm compared with the maxima of **4** and **5**, possibly due to the structural asymmetry induced by trimethylsilyl and decreased conjugation in complexes of **1** and **2**. While emission maxima of complex **3** is red-shifted by 19 nm, compared with the maxima of **6**. Based on the PL data in powder state at 297 K, the Commission Internationale de L'Eclairage color coordinates are (0.2073, 0.3429), (0.2440, 0.4409), (0.3629, 0.5147), (0.2922, 0.4163), (0.3528, 0.4828) and (0.3023, 0.4864) for **1-6**, respectively (Fig.5). Based on the optimized S_1 geometries of these complexes, the emission properties were also estimated using the TDDFT method. The calculated emission wavelengths of **1-6** (Table 4) agree well with the experimental ones, suggesting the reliability of our TDDFT method. The main contribution to the emission is identified as the LUMO⇒HOMO transition. Based on the S_1 state geometry, the contour plots of the HOMO and LUMO are shown in Fig.6. The LUMO is mainly confined to Cu and X and phosphorus in dpts, and the HOMO is mainly focused on the thioenyl rings in dpts. So, the luminescence mainly originates from MLCT, XLCT and intraligand transitions.

At 77 K, the emission maxima of complexes **1-6** are between 473 and 536 nm. Compared to room temperature, except **3**, the emission bands of complexes **1-2** and **4-6** are blue-shifted because the suppression of the excited state energy relaxation

caused by structural changes involving vibrations and rotations[23].The emission band of complex **3** is red-shifted because the thermal population of a lower excited state (T_1) dominates at low temperature [23]. The lifetimes of luminescence at 297 K for **1-3** are 2~110 times shorter than those at 77 K (Table 4, Figs.S26-37), indicating that the complexes may contain different emissive processes that are inter-exchangeable and thermally activated [36]. The S_1 and T_1 energy levels are estimated according to the fluorescence and phosphorescence spectra onsets (Table 4, Fig.4). The resulted slight $\Delta E(S_1-T_1)$ values (0.0575~0.1283 eV) matches well with the $\Delta E^{adi}(S_1-T_1)$ values (0.0610~0.1166 eV) by TDDFT calculations, indicating that complexes **1–6** can show a very efficient thermally activated delayed fluorescence [37] (Table 4). The radiative rate constant k_r of complexes **1-6** was calculated to be $6.2 \times 10^3 \sim 2.04 \times 10^4$ s^{-1}, 1~2 orders of magnitude larger than those Cu(I) halide complexes with dimethylthiophene diphosphine ligand dpmt and PPh_3 [33b], which are due to the much shorter lifetimes of the complexes.

To prove the existence of these thermally equilibrated emitting states, we selected complex **2** as a representative example, the observed decay time (τ_{obs}) as a function of temperature in the range between 77 K and 317 K is obtained in Fig.7. When the exciton population is assumed to be in thermal equilibrium among the excited states, the observed decay time can be expressed as a function of the temperature according to eqn (1) that has been found in the literature [38].

$$\tau_{obs} = \frac{1 + \frac{1}{3}\exp\left(-\frac{\triangle E_{ST}}{K_B T}\right)}{\frac{1}{\tau(T_1)} + \frac{1}{3\tau(S_1)}\exp\left(-\frac{\triangle E_{ST}}{K_B T}\right)} \quad (1)$$

In this equation, K_B and T represent the Boltzmann constant and the absolute temperature, respectively. $\tau(S_1)$ and $\tau(T_1)$ are the emission decay times of S_1 and T_1, and ΔE_{ST} is the energy separation between these two states. Because in the temperature range investigated a single-exponential decay behavior was found, it can be concluded that a fast thermalization between S_1 and T_1. Fitting eqn (1) to the measured decay time data at different temperatures, the parameters were obtained with values of $\tau(S_1)$ = 0.9361 μs, $\tau(T_1)$ = 579.3 μs, and ΔE_{ST} = 0.0798 eV. The short decay time of 0.9361 μs determined for the thermally activated state substantiates its singlet character. Thus, the measured emission decay time at 297 K of τ = 48.9 μs represents a delayed fluorescence. It is remarked that despite this short decay time of the singlet state, no spontaneous fluorescence is directly observed. This indicates that the intersystem crossing (ISC) from the S_1 to T_1 state, is much faster than the prompt $S_1 \rightarrow S_0$ emission. The fitted (T_1) value approximate to the decay time 595 μs for **2** observed at 77 K, and the obtained energy difference ΔE_{ST} is close to the value 0.1000 eV calculated the energy gap between the adiabatic excitation energies S_1 and T_1. As shown in Fig.7, the solid fitting curve matches well with the experimental data. At low temperatures (below 97 K), a nearly constant value of ca. 580 μs is observed for complex **2**, indicating that the exciton population is predominantly frozen in the T_1 state, and thus complex **2** emits almost pure phosphorescence at such low

temperatures. With the temperature increases, the intensity contributed from the T_1 state decreases, while the intensity stemming from the S_1 state (TADF) increases, which due to the small energy gap between S_1 and T_1. We evaluated the temperature-dependent relative contributions of TADF and phosphorescence in the overall emission [36]. Applying eqn (2) and (3) and using the fit parameters as determined for complex **2** (ΔE_{ST} = 0.0798 eV, $\tau(S_1)$ = 0.9361 μs, $\tau(T_1)$ = 579.3 μs, $\Phi_{PL}(S_1)$ = 0.52, and $\Phi_{PL}(T_1)$ = 0.87), the plots showing in Fig.8 are obtained. As depicted in Fig.8, at room temperature, the phosphorescence and TADF account for 16% and 84% for complex **2**, respectively.

$$\frac{I(T_1)}{I_{tot}} = \left[1 + \frac{\Phi_{PL}(S_1)\tau(T_1)}{3\Phi_{PL}(T_1)\tau(S_1)} e^{-\triangle E_{ST}/K_B T} \right]^{-1} \quad (2)$$

$$\frac{I(S_1)}{I_{tot}} = 1 - \left[1 + \frac{\Phi_{PL}(S_1)\tau(T_1)}{3\Phi_{PL}(T_1)\tau(S_1)} e^{-\triangle E_{ST}/K_B T} \right]^{-1} \quad (3)$$

The selected bond lengths and angles in the optimized S_0, S_1, and T_1 geometries for complexes **1-6** are collected in Table S1. The core structures in the optimized S_0, S_1, and T_1 geometries for complexes **1-6** are shown in Fig.S45. The S_1 and T_1 coordination geometries of the copper center of **1–6** are highly distorted tetrahedral. For complexes **1-3**, smaller changes of P1-Cu-P2, P2-Cu-P3 and P3-Cu-X bond angles in comparison to the ground state (S_0), which result in much higher quantum efficiencies than complexes **4-6**. These bond angels changes possibly results in some nonradiative processes cause by Jahn-Teller distortion of emissive excited states [24]

and not very high quantum efficiency in complexes **4-6**, due to no bulky trimethylsililyl group near to P1 atom.

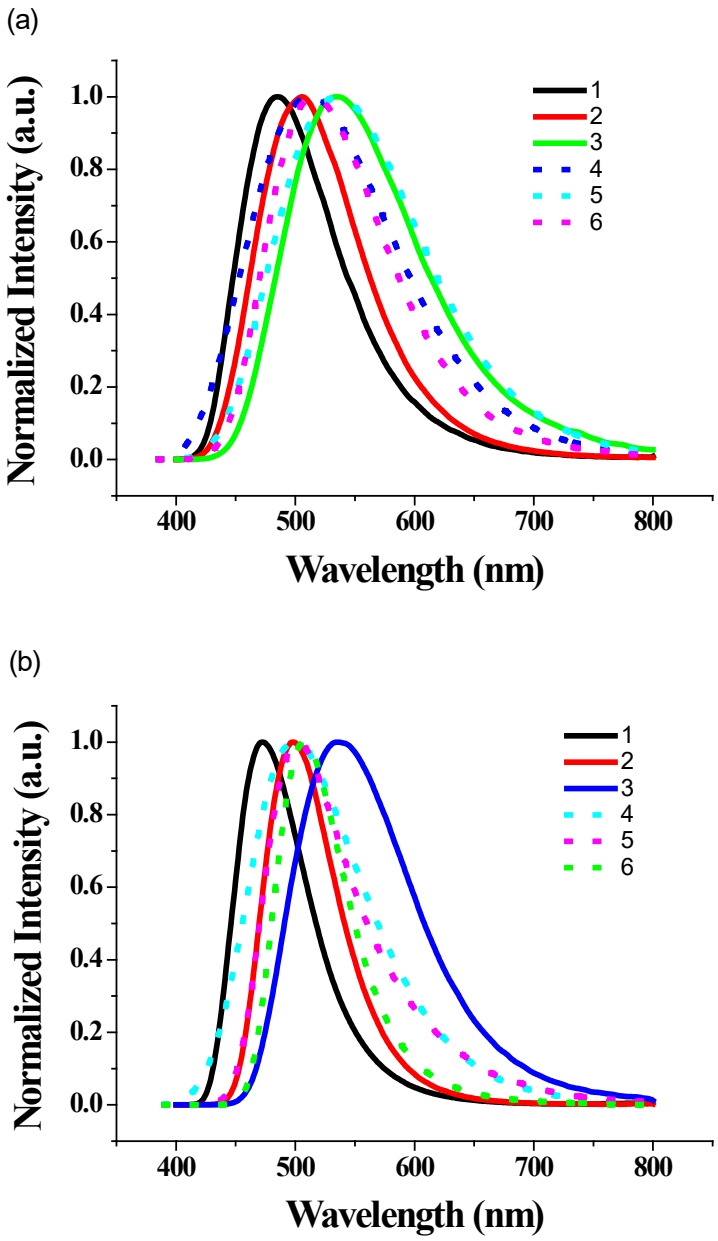

Fig.4. Normalized emission spectra of complexes **1–6** in powder state at (a) 297 K and (b) 77 K.

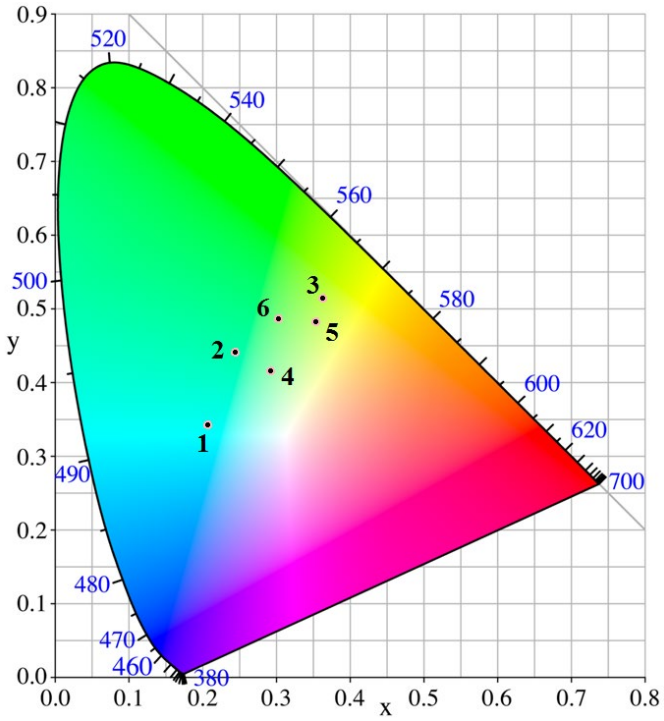

Fig.5. CIE graph of complexes **1–6**.

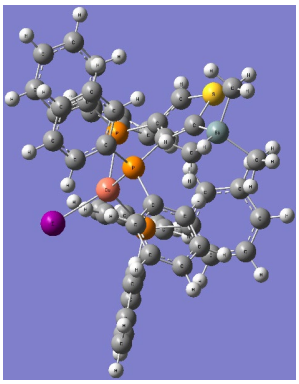

The optimized S_1 geometry

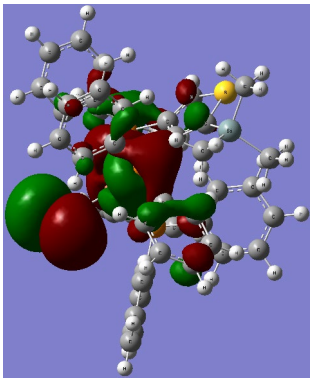

HOMO E = –4.74 eV

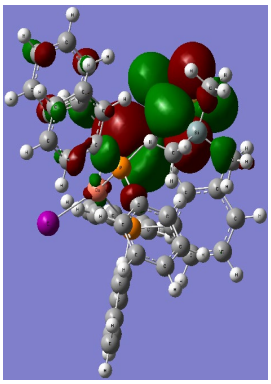

LUMO E = –2.18 eV

1

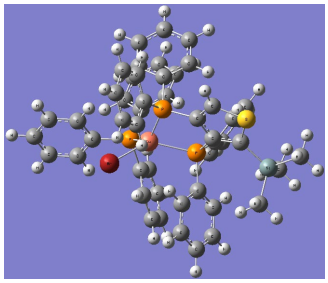

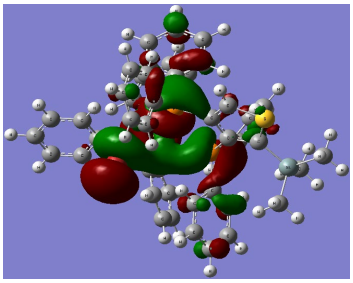

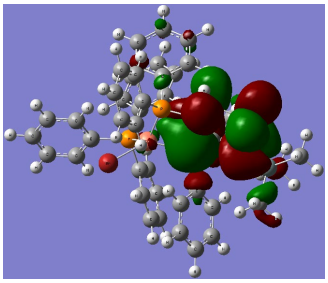

The optimized S_1 geometry HOMO E = –4.57 eV LUMO E = –2.11 eV

2

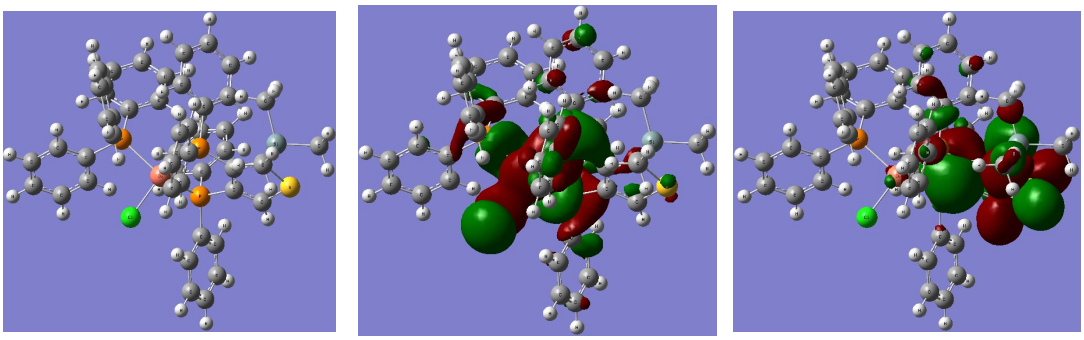

The optimized S_1 geometry HOMO E = –4.64 eV LUMO E = –2.10 eV

3

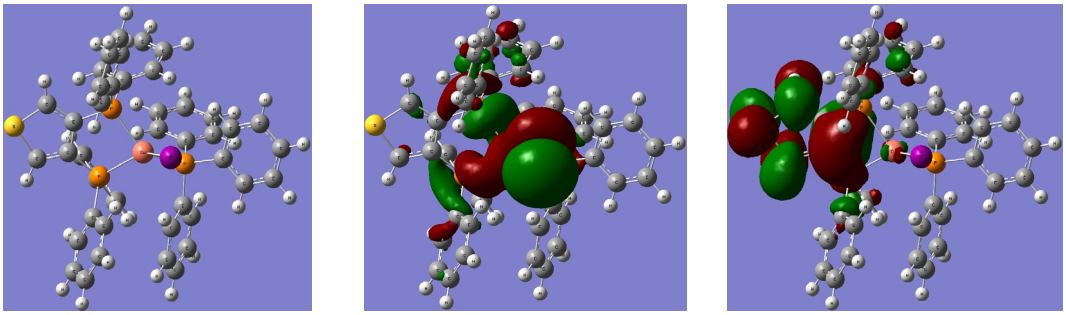

The optimized S_1 geometry HOMO E = –4.56 eV LUMO E = –2.02 eV

4

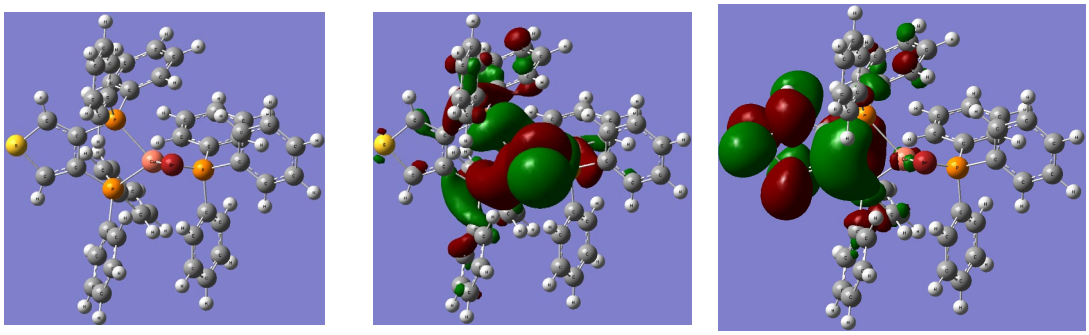

The optimized S_1 geometry HOMO E = –4.58 eV LUMO E = –1.99 eV

5

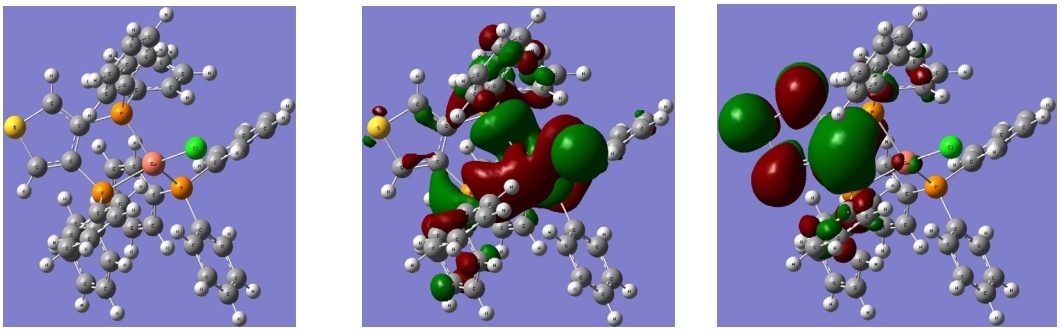

The optimized S_1 geometry HOMO E = –4.50 eV LUMO E = –2.02 eV

6

Fig.6. The optimized S_1 geometry, electron cloud distribution of HOMO and LUMO at S_1 geometry for complexes **1–3**.

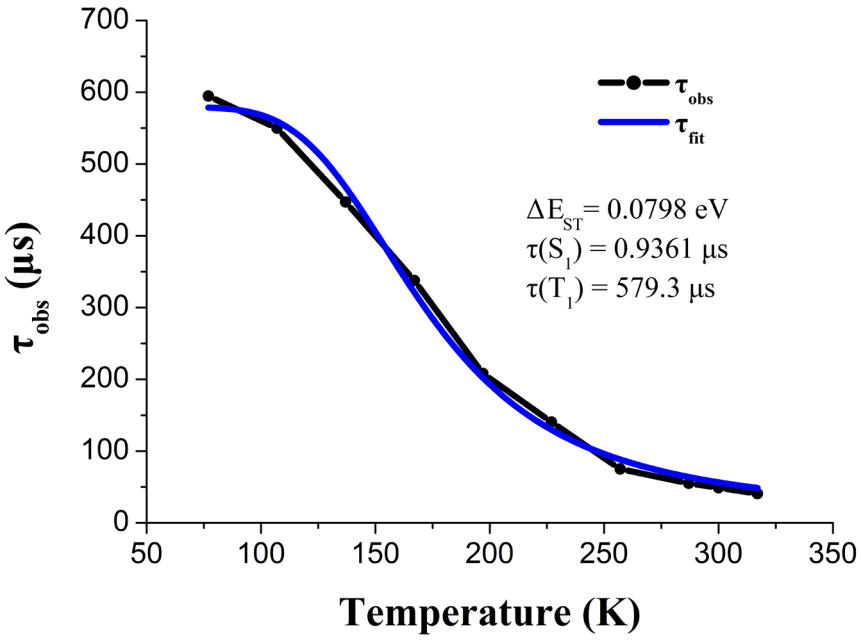

Fig.7. Temperature dependence of decay time for complex **2** in powder state and fitting curve (the inset shows the fitting parameters).

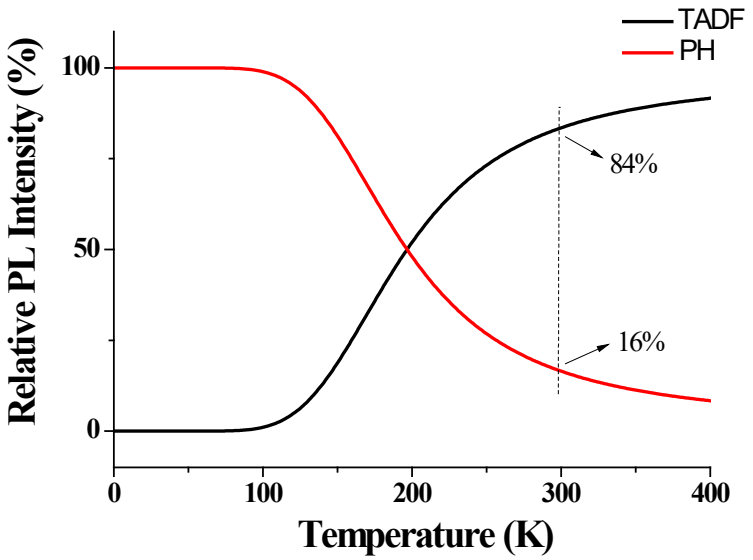

Fig.8. The contributions of TADF and phosphorescence to the luminescence of complex **2** in powder state as a function of temperature.

Table 4. Photophysical data of **1–6** in powder state.

	λ_{max} (nm)[a]		τ_{ave} (μs)[b]		Φ_s[c]	k_r[d] (10^4 s^{-1})	$E^{adi}(S_1)$ (eV)[e]	$E^{adi}(T_1)$ (eV)[e]	ΔE^{adi} (S_1-T_1) (eV)[e]	λ (nm)[f]
	297 K	77 K	297 K	77 K	297 K	297 K				
1	485	473	36.4	73.9	0.41	1.13	2.4381	2.3327	0.1054	508
							3.0542 [g]	2.9952 [g]	0.0590 [g]	
2	506	498	48.9	595	0.52 (0.87*)	1.06	2.6176	2.5176	0.1000	473
							3.0318 [g]	2.9040 [g]	0.1278 [g]	
3	535	536	20.8	772	0.29	1.39	2.6223	2.5057	0.1166	472
							2.9594 [g]	2.8311 [g]	0.1283 [g]	
4	515	499	9.0	108	0.18	2.04	2.6788	2.6133	0.0655	463
							3.2208 [g]	3.1633 [g]	0.0575 [g]	
5	535	502	10.0	469	0.07	0.65	2.7460	2.6661	0.0799	452

							3.0923 [g]	2.9880 [g]	0.1043 [g]	
6	516	508	4.2	462	0.03	0.62	2.5689	2.5079	0.0610	483
							3.0024 [g]	2.8972[g]	0.1052 [g]	

[a] Emission peak wavelength.

[b] Averge lifetime was used and calculated by the equation $\tau_{ave} = \Sigma A_i T_i^2/\Sigma A_i T_i$, A_i and T_i are shown in Figures S26-S37. Experimental errors are ± 5%.

[c] Absolute emission quantum in air. Asterisk indicates at 77 K. Experimental errors are ± 5%.

[d] Radiative decay rate. $k_r = \Phi/\tau_{ave}$.

[e] $E^{adi}(S_1)$ and $E^{adi}(T_1)$ are the adiabatic excitation energies, which correspond to the $S_0 \rightarrow S_1$ and $S_0 \rightarrow T_1$ transitions, respectively. The energy gap between S_1 and T_1 is then obtained through $\Delta E^{adi}(S_1–T_1) = E^{adi}(S_1)– E^{adi}(T_1)$.

[f] Calculated emission wavelengths based on the optimized S_1 geometries.

[g] The S_1 and T_1 energy levels were estimated according to the emission peak onsets at 297 K and 77 K.

3.4.Thermal properties

Since good thermal stabilities of the complexes are important for OLED applications, the onset decomposition temperatures (T_{dec}) of complexes **1-6** were determined by thermogravimetric analysis (TGA) under a stream of nitrogen. From the onset of the TGA curves (Fig. 9), all complexes show good thermal stabilities with their T_{dec} values ranging from 229 to 264 °C for complexes **1-6**. The first-step weight loss for complex **3** of ca. 39 % was observed at 300 °C, ca. 37~43% was observed between 390 and 430 °C for complexes **4-6**, which is due to the removal of halogen and PPh_3. The second-step weight loss was observed at 352 °C for complex **3**, and from 472 to 476 °C for complexes **4-6**, which can be ascribed to the removal or

decomposition of dpts. The weight loss for complexes **1** and **2** of ca. 80~88 % was observed at 475 °C, which is due to the removal of halogen, PPh_3 and dpts.

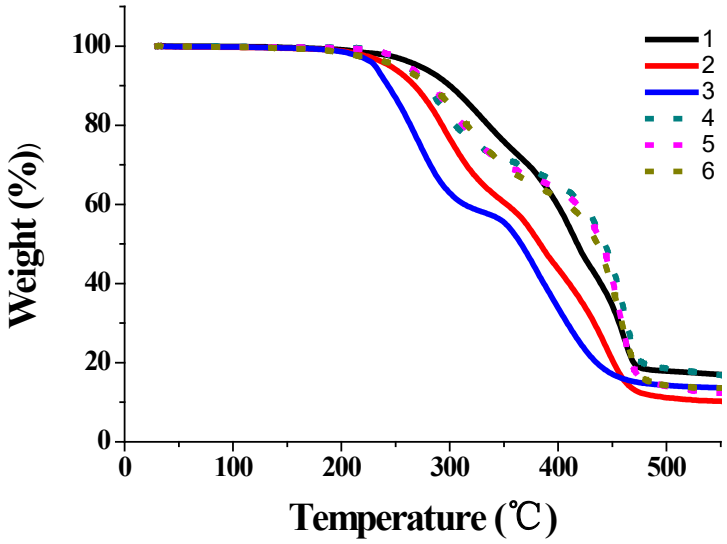

Fig. 9. TGA traces of complexes **1–6**.

3.5.Device performance

Solution-processed devices based on complex **2** were fabricated with the structure of ITO/ PEDOT:PSS (40 nm)/ complex **2** (30 nm)/ TPBi (30 nm)/ LiF (1 nm)/ Al (100 nm). In the device, ITO (indium tin oxide) was used as the anode, PEDOT: PSS (Poly(3,4-ethylenedioxythiophene)：poly(styrenesulfonate)) used as hole injection layer, complex **2** used as the EML, 1,3,5-Tris(1-phenyl-1H-benzimidazol-2-yl)benzene (TPBi) used as the electron transporting layer, LiF served as electron injecting layer and Al as cathode. The energy level diagram of the device is shown in Fig.10(a). This device exhibits yellow green emission at 564 nm with CIE (x, y) of (0.43, 0.51). The EL spectrum of the device is shown in Fig.10(b). The device gives maximum external quantum efficiency

(EQE) of 7.74% and presented maximum luminance of 234 cd/m^2. As far as we know, this value of EQE and luminance is the highest among the previously reported solution-processed OLEDs fabricated with neutral mononuclear Cu(I) halide complexes. In addition, we fabricated several doped devices with CBP (1,3-bis(9-carbazolyl)benzene) and mCP (4,4'-bis(9-carbazolyl)biphenyl) as host materials. The doped devices didn't perform as well as the non-doped device (Fig. S46-S47). The unsatisfactory performance of the doped devices may be due to the defective energy level matching between CBP, mCP and complex **2**. A more suitable host material is needed to improve device performance with complex **2**.

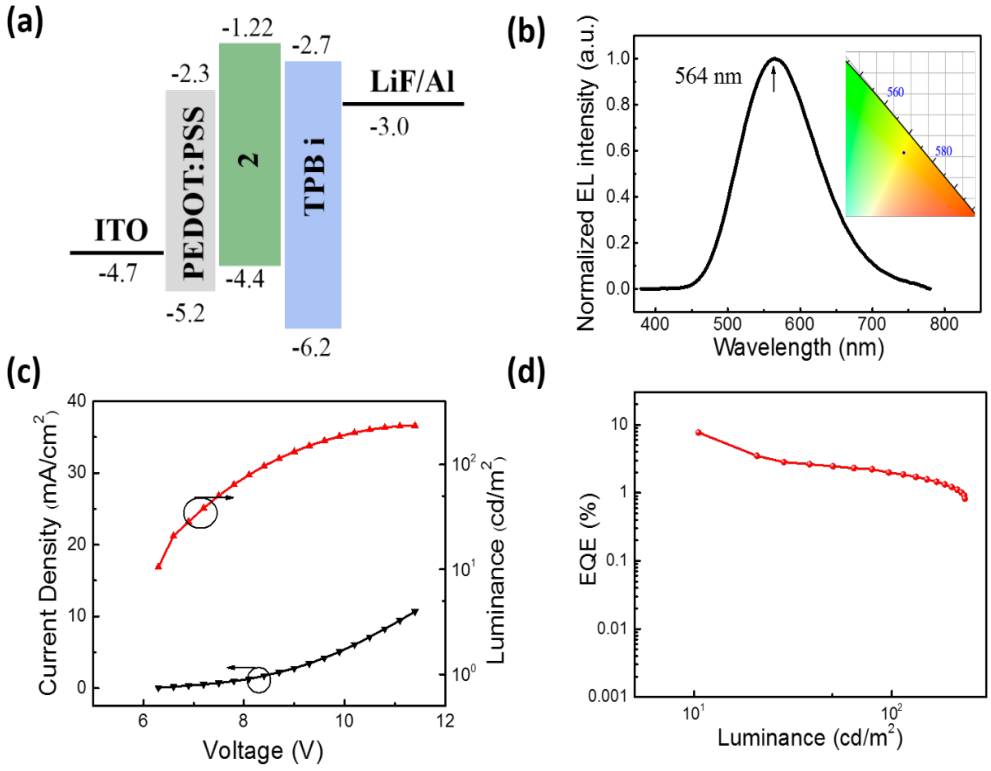

Fig. 10. (a) Energy-level diagram of the device based on the complex **2**; (b) EL spectra, and the inset is the CIE of EL spectra; (c) Current density-voltage-luminance (J-V-L) characteristics; (d) EQE-luminance characteristics.

4. Conclusions

This is the first report on efficient TADF-OLEDs with ultra-soluble Cu(I) halide complexes containing non-symmetrically substituted bidentate phosphine and PPh_3 ligands. The nondoped device gives a maximum external quantum efficiency (EQE) of 7.74 % and a maximum luminance of 234 cd/m^2 with CIE(x,y) of (0.43, 0.51). This value of EQE and luminance is the highest among the previously reported solution-processed OLEDs fabricated with neutral mononuclear Cu(I) halide complexes. The introduction of bulky and flexible trimethylsilyl group into diphosphine ligand, not only greatly improves the solubility of the complexes, but also quantum efficiency, which is due to the suppression of nonradiative processes caused by Jahn-Teller distortion of emissive excited states, and fine-tunes the emission color as well. This provides a strategy for making ultra-soluble TADF materials to allow the solution-processed devices, high-performance inks that can be adjusted to various print heads by using solvent mixtures with tailor-made viscosity and surface tension properties.

Conflicts of interest

There are no conflicts to declare.

Acknowledgements

This work was supported by the National Natural Science Foundation of China [grant

number 21671061] and application foundation frontier special project by Wuhan Science and Technology Bureau [grant number 2019010701011414]. We thank senior engineer Mingxing Chen (Peking University) for his measurement of photoluminescence property of complexes.

Reference

[1] Yersin H, Rausch AF, Czerwieniec R, Hofbeck T, Fischer T. Triplet harvesting and singlet harvesting for efficient OLEDs. Coord Chem Rev 2011;255(21): 2622-2652.

[2] Lin CH, Hsu CW, Liao JL, Cheng YM, Chi Y, Lin TY, Chung MW, Chou PT, Lee GH, Chang CH, Shih CY, Ho CL. Phosphorescent OLEDs assembled using Os(II) phosphors and a bipolar host material consisting of both carbazole and dibenzophosphole oxide. J Mater Chem 2012;22:10684.

[3] Kessler F, Costa RD, Censo DDi, Scopelliti R, Orti E, Bolink HJ, Meier S, Sarfert W, Gratzel M, Nazeeruddin MK, Baranoff E. Near-UV to red-emitting charged bis-cyclometallated iridium(III) complexes for light-emitting electrochemical cells. Dalton Trans 2012;41(1): 180-191.

[4] Baranoff E, Fantacci S, Angelis FDe, Zhang X, Scopelliti R, Gratzel M, Nazeeruddin MK. Cyclometalated Iridium(III) complexes based on phenyl-Imidazole ligand. Inorg Chem 2011;50(2): 451-462.

[5] Wallesch M, Volz D, Zink DM, Schepers U, Nieger M, Baumann T, Bräse S. Bright coppertunities: multinuclear CuI complexes with N–P ligands and their applications. Chem Eur J 2014;20(22): 6578-6590.

[6] Gong X, Ostrowski JC, Bazan GC, Moses D, Heeger AJ, Red electrophosphorescence from polymer doped with iridium complex. Appl Phys Lett 2002;81(20): 3711-3713.

[7] Welter S, Brunner K, Hofstraat JW, Cola LDe. Electroluminescent device with reversible switching between red and green emission. Nature 2003;421(6918): 54-57.

[8] Cuttell DG, Kuang SM, Fanwick PE, McMillin DR, Walton RA. Simple Cu(I) complexes with unprecedented excited-state lifetimes. J Am Chem Soc 2002;124(1): 6-7.

[9] Kuang SM, Cuttell DG, McMillin DR, Fanwick PE, Walton RA. Synthesis and structural characterization of Cu(I) and Ni(II) complexes that contain the bis[2-(diphenylphosphino)phenyl]ether ligand novel emission properties for the Cu(I) species. Inorg Chem 2002;41(12): 3313-3322.

[10] Wang YM, Teng F, Hou YB, Xu Z, Wang YS, Fu WF. Copper(I) complex employed in organic light-emitting electrochemical cells: device and spectra shift. Appl Phys Lett 2005;87(23): 233512.

[11] McCormick T, Jia WL, Wang S, Phosphorescent Cu(I) complexes of 2-(2'-pyridylbenzimidazolyl)benzene: impact of phosphine ancillary ligands on

electronic and photophysical properties of the Cu(I) complexes. Inorg Chem 2006;45(1): 147-155.

[12] Jia WL, MCormick T, Tao Y, Lu JP, Wang SN. New phosphorescent polynuclear Cu(I) compounds based on linear and star-shaped 2-(2'-pyridyl)benzimidazolyl derivatives: syntheses, structures, luminescence, and electroluminescence. Inorg Chem 2005;44(16): 5706.

[13] Pawlowski V, Knör G, Lennartz C, Vogler A. Luminescence and theoretical studies of Cu(tripod)X [tripod = 1,1,1-tris(diphenylphosphanylmethyl)ethane; X- = halide, thiophenolate, phenylacetylide]. Eur J Inorg Chem 2005;15: 3167-3171.

[14] Maini L, Braga D, Mazzeo PP, Ventura B. Polymorph and isomer conversion of complexes based on CuI and PPh_3 easily observed via luminescence. Dalton Trans 2012;41: 531-539.

[15] Tung YL, Lee SW, Chi Y, Chen LS, Shu CF, Wu FI, Carty AJ, Chou PT, Peng SM, Lee GH. Organic light-emitting diodes based on charge-neutral RuII phosphorescent emitters. Adv Mater 2005;17(8):1059-1064.

[16] Tsuboyama A, Kuge K, Furugori M, Okada S, Hoshino M, Ueno K. Photophysical properties of highly luminescent copper(I) halide complexes chelated with 1,2-bis(diphenylphosphino)benzene. Inorg Chem 2007;46: 1992-2001.

[17] Uoyama H, Goushi K, Shizu K, Nomura H, Adachi C. Highly efficient organic light-emitting diodes from delayed fluorescence. Nature 2012;492(7428):234-238.

[18] Zhang Q, Zhou Q, Cheng Y, Wang L, Ma D, Jing X, Wang F. Highly efficient green phosphorescent organic light-emitting diodes based on CuI complexes. Adv Mater 2004;16(5): 432-436.

[19] Adachi C. Third-generation organic electroluminescence materials. Jpn J Appl Phys 2014;53: 060101.

[20] Wei F, Qiu J, Liu X, Wang J, Wei H, Wang Z, Liu Z, Bian Z, Lu Z, Zhao Y, Huang C. Efficient orange-red phosphorescent organic light-emitting diodes using an in situ synthesized copper(I) complex as the emitter. J Mater Chem C 2014;2(31):6333-6341.

[21] Xu H, Chen R, Sun Q, Lai W, Su Q, Huang W , Liu X. Recent progress in metal–organic complexes for optoelectronic applications. Chem Soc Rev 2014;43:3259-3302.

[22] Zhang J, Duan C, Han C, Yang H, Wei Y, Xu H. Balanced dual emissions from tridentate phosphine‐coordinate copper(I) complexes toward highly efficient yellow OLEDs. Adv Mater 2016;28(28):5975-5979.

[23] Osawa M, Hoshino M, Hashimoto M, Kawata I, Igawa S, Yashima M. Application of three-coordinate copper(I) complexes with halide ligands in organic light-emitting diodes that exhibit delayed fluorescence. Dalton Trans 2015;44(18):8369-8378.

[24] Hashimoto M, Igawa S, Yashima M, Kawata I, Hoshino M, Osawa M. Highly efficient green organic light-emitting diodes containing luminescent tetrahedral

copper(I) complexes. J Am Chem Soc 2011;133(27):10348-10351.

[25] Jiao B, Wang J, Huang J, Cao M, Liu C, Yin G, Zhu Y, Zhang B, Du C. Design and synthesis of stable cuprous complexes bearing P^N-type ligands for vapor-deposited organic light-emitting device. Org Electron 2019;64, 158-165.

[26] Xie M, Han C, Zhang J, Xie G, Xu H. White electroluminescent phosphine-chelated copper nanoclusters. Chem Mater 2017;29(16): 6606-6610.

[27] Zhang, Komino T, Huang S, Matsunami S, Coushi K, Adachi C. Triplet exciton confinement in green organic light‐emitting diodes containing luminescent charge‐transfer Cu(I) complexes. Adv Funct Mater 2012;22(11):2327-2336.

[28] Volz D, Chen Y, Wallesch M, Liu R, Fléchon C, Zink DM, Friedrichs J, Flügge H, Steininger R, Göttlicher J, Heske C, Weinhardt L, Bräse S, So F, Baumann T. Bridging the efficiency gap: fully bridged dinuclear Cu(I)-complexes for singlet harvesting in high-efficiency OLEDs. Adv Mater 2015;27(15):2538-2543.

[29] Verma A, Zink DM, Fléchon C, Carballo JL, Flügge H, Navarro JM, Baumann T, Volz D. Efficient, inkjet-printed TADF-OLEDs with an ultra-soluble NHetPHOS complex. Appl Phys A 2016;122(3):191.

[30] Wallesch M, Verma A, Fléchon C, Flügge H, Zink DM, Seifermann SM, Navarro JM, Vitova T, Göttlicher J, Steininger R, Weinhardt L, Zimmer M, Gerhards M, Geske C, Bräse S, Baumann T, Volz D. Towards printed organic light-emitting devices: a solution-stable, highly soluble Cu(I)-NHetPHOS-complex for inkjet processing. Chem Eur J 2016;22(46):

16400-16405.

[31] Volz D, Zink DM, Bocksrocker T, Friedrichs J, Nieger M, Baumann T, Lemmer U, Bräse S. Molecular construction kit for tuning solubility, stability and luminescence properties: heteroleptic MePyrPHOS-copper Iodide-complexes and their application in organic light-emitting diodes chemistry of materials. Chem Mater 2013;25(17): 3414-3426.

[32] Zink DM, Volz D, Baumann T, Mydlak M, Flügge H, Friedrichs J, Nieger M, Bräse S. Heteroleptic, dinuclear copper(I) complexes for application in organic light-emitting diodes. Chem Mater 2013;25(22): 4471-4486.

[33](a) Wei Q, Chen HT, Liu L, Zhong XX, Wang L, Li FB, Cong HJ, Wong WY, Alamry KA, Qin HM. Syntheses and photoluminescence of copper(I) halide complexes containing dimethylthiophene bidentate phosphine ligands. New J Chem 2019;43:13408-13417; (b) Wei Q, Zhang R, Liu L, Zhong XX, Wang L, Li GH, Li FB, Alamry KA, Zhao Y. From deep blue to green emitting and ultralong fluorescent copper(I) halide complexes containing dimethylthiophene diphosphine and PPh_3 ligands. Dalton Trans 2019;48(30): 11448-11459; (c) Liu LP, Zhang R, Liu L, Zhong XX, Li FB, Wang L, Wong WY, Li GH, Cong HJ, Alharbi NS, Zhao Y. A new strategy to synthesize three-coordinate mononuclear copper(I) halide complexes containing a bulky terphenyl bidentate phosphine ligand and their luminescent properties. New J Chem 2019;43:3390-3399; (d) Liu LP, Li Q, Xiang SP, Liu L, Zhong XX, Liang C, Li GH, Hayat T, Alharbi NS, Li FB, Zhu

NY, Wong WY, Qin HM, Wang L. Near-saturated red emitters: four-coordinate copper(I) halide complexes containing 8-(diphenylphosphino)quinoline and 1-(diphenylphosphino)naphthalene ligands. Dalton Trans 2018;47:9294-9302; (e) Zhang WJ, Zhou ZX, Liu L, Zhong XX, Asiri AM, Alamry KA, Li FB, Zhu NY, Wong WY, Qin HM. Highly-efficient blue neutral mononuclear copper(I) halide complexes containing bi- and mono-dentate phosphine ligands. J Lumin 2018;196:425-430; (f) Li Q, Xie P, Liu L, Zhong XX, Asiri AM, Alamry KA, Li FB, Zhu NY, Wong WY, Qin HM. Synthesis, characterization and luminescent properties of three-coordinate copper(I) halide complexes containing a carbazolyl monodentate phosphine ligand. J Coord Chem 2018;71:4072-4085.

[34] Zhang C, Song L, Wu H, Ji X, Jiao J, Zhang J. Ethylene tri-/tetramerization catalysts supported by diphosphinothiophene ligands. Dalton Trans 2017;46:8399-8404.

[35] Clifton J, Habraken ERM, Pringle PG, Manners I. Subtle effects of ligand backbone on the efficiency of iron-diphos catalysed negishi cross-coupling reactions. Catal Sci Technol 2015;5:4350-4353.

[36] Leitl MJ, Küchle FR, Mayer HA, Wesemann L, Yersin H. Brightly blue and green emitting Cu(I) dimers for singlet harvesting in OLEDs. J Phys Chem A 2013;117(46):11823.

[37] Kang L, Chen J, Teng T, Chen XL, Yu R, Lu CZ. Experimental and theoretical studies of highly emissive dinuclear Cu(I) halide complexes with delayed

fluorescence. Dalton Trans 2015; 44: 11649-11659.

[38] Yersin H, Czerwieniec R, Hupfer A. Singlet harvesting with brightly emitting Cu(I) and metal-free organic compounds. Proc SPIE 2012;8435(6):2.